

Contrasting properties of gold nanoshells and titanium dioxide nanoparticles for optical coherence tomography imaging of skin: Monte Carlo simulations and *in vivo* study

Mikhail Kirillin

Institute of Applied Physics of the Russian Academy of Sciences
603950 Ulyanov Street
46, Nizhny Novgorod
Russia

Marina Shirmanova

Marina Sirotkina

Marina Bugrova

Nizhny Novgorod State Medical Academy
603005, Minin and Pozharsky Square
10/1, Nizhny Novgorod
Russia

Boris Khlebtsov

Institute of Biochemistry and Physiology of Plants and Microorganisms of the Russian Academy of Science
410049, pr. Entuziastov
13, Saratov
Russia

Elena Zagaynova

Nizhny Novgorod State Medical Academy
603005, Minin and Pozharsky Square
10/1, Nizhny Novgorod
Russia

Abstract. The effect of silica/gold nanoshells and titanium dioxide nanoparticles on the optical properties of skin is studied. By implementing *in vivo* measurements and Monte Carlo simulations, we analyze the efficiency of using these nanoparticles as contrasting agents for optical coherence tomography (OCT) imaging of skin. *In vivo* measurements are performed on pig skin, where nanoparticle suspension drops have been applied. The identification of skin layers is performed by comparison with corresponding histology images. Experimental results exhibit an increase in contrast of the obtained OCT images after a single nanoparticles application. Multiple applications do not lead to increase in the obtained contrast. To interpret the obtained experimental OCT images of skin and understand the mechanisms of contrasting, a set of Monte Carlo calculations is performed. The results of the simulations exhibit good qualitative agreement with the experimental images, and prove that the contrasting originates from the nanoparticles added, while the contrast of inclusion originates from the absence of nanoparticles within it and their presence in the surrounding area. © 2009 Society of Photo-Optical Instrumentation Engineers. [DOI: 10.1117/1.3122373]

Keywords: optical coherence tomography; skin; nanoparticles; contrasting; Monte Carlo simulations.

Paper 08209SSR received Jul. 4, 2008; revised manuscript received Dec. 22, 2008; accepted for publication Mar. 19, 2009; published online Apr. 23, 2009.

1 Introduction

Optical coherence tomography (OCT) is a noninvasive technique for imaging biotissues at a depth of up to 2 mm with axial spatial resolution down to units of micrometers based on low-coherent interferometry in the near-infrared (NIR) range of wavelengths ($\lambda=0.75\text{--}1.3\ \mu\text{m}$).^{1–3} In recent years, OCT proved to be an efficient tool for *in vivo* imaging of superficial tissues of skin and mucous membranes.^{4,5} However, multiple light scattering in skin originating from optical nonuniformities limits significantly the imaging depth of OCT and contrasting of the forming elements within the studied medium.⁶

Traditionally when imaging biotissues, osmotically active immersion liquids such as glycerol, propylene glycol, dextrans, and concentrated glucose solutions are administered to the sample under study to decrease the effect of multiple scattering.^{7,8} This administration known as optical clearing is based on the fact that a medium with refractive index value close to that of the components of the scattering media substitutes the medium with a significantly different refractive

index. The substitution changes the scattering properties of the object under study,^{9,10} thus decreasing the scattering coefficient and increasing the anisotropy factor. However, for backscattering detection techniques, administration of optical clearing agents leads to decrease in intensity contributing to the signal, which can provide negative effects on the sensitivity of the technique. The essential requirements for potential contrasting agents are the ability to penetrate into the skin after superficial administration and chemical inactivity.

The efficiency of using gold nanoparticles as a contrast agent for optical imaging of cells and tissue phantoms has been demonstrated for colloidal gold,¹¹ nanoparticle clusters,¹² nanoshells with nucleus/coating structures,^{5,13} nanorods,¹⁴ nanocages,¹⁵ and others. The advantages of gold nanoparticles are low toxicity and the ability for maintenance of localized surface plasmon resonances in the NIR region,^{14,16} providing enhanced backscattering of probing radiation. The nanoshells with silica nucleus and gold coating appear to be the best perspective for contrasting of OCT images of biotissues due to the fact that the wavelengths of plasmon resonances they maintain are within the so-called

Address all correspondence to Mikhail Kirillin, Laboratory of Biophotonics, Institute of Applied Physics RAS, Ulyanov str. 46, Nizhny Novgorod, 603950 Russia; Tel: 7 831 4164619; Fax: 7 831 4363792; E-mail: mkirillin@yandex.ru

“transparency window” ($\lambda=0.6\text{--}1.3\ \mu\text{m}$). By varying such geometrical parameters as size and nucleus/coating radius ratio of the nanoshells, one can control the wavelength of the plasmon resonance and obtain the particles with preset optical properties.^{17,18} It was demonstrated earlier that gold nanoparticles, in particular gold nanoshells, are used to enhance contrast of optical images of biological tissues. Lee et al. traced the enhancement of contrast and depth of OCT images of mouse liver *ex vivo* on intravenous injection of gold nanoparticles.¹⁹ Gobin et al. intravenously injected gold nanoshells (the concentration of nanoparticles was 1.5×10^{10} particles/ml) in mice with grafted tumors. Accumulation of nanoparticles in the tumor was maximal in 20 h, and the signal from this zone of the OCT image was increased.²⁰ Our preliminary studies of gold nanoshells on agar phantoms and rabbit skin also demonstrated that gold nanoshells provide contrasting effects on OCT images.^{5,21}

Other potential contrasting agents are titanium dioxide (TiO_2) nanoparticles, widely used in cosmetic production,^{22,23} for protection against detrimental effects of UV radiation. These particles were also supposed to be effective contrast agents for OCT imaging due to high scattering properties and comparatively low absorption in the NIR range, in particular for 800 nm.¹⁵ TiO_2 nanoparticles have a tendency toward aggregates and agglomerates formation, which leads to a shift of maximum scattering efficiency to the visible range.²⁴ Experimentally the contrasting effect of these nanoparticles was proved in Ref. 25 on water suspensions and turbid tissue-mimicking phantoms. In Ref. 26, the authors show that particles penetrate into skin at a depth not more than $3\ \mu\text{m}$ and absorb UV radiation. The possibility of nanoparticles penetrating into skin during surface application is currently discussed. The authors of some works argue against nanoparticles penetration into skin. For example, in Ref. 27, $4\ \text{mg}/\text{cm}^2$ of sunscreen containing titanium dioxide nanoparticles (10 to 100 nm) was applied to human skin and it was shown that titanium dioxide nanoparticles do not penetrate into deep skin layers: epidermis and dermis. However, the nanoparticles may penetrate through intracellular space, through cells, or skin appendages (hair follicles and sebaceous and sweat glands).²⁸

Nevertheless, *in vivo* experimental data available are insufficient for developing an appropriate procedure for increasing contrast and imaging depth provided by an OCT system for both types of nanoparticles. When applying nanoparticles as contrasting agents in OCT, one should be sure that the effect is provided exactly by nanoparticles and that they do not affect structural properties of the object under study. In *in vivo* studies, it is difficult to control these properties during the experiment. On the other side, theoretical calculations of the obtained OCT signals and images are impossible due to complicated geometry of the skin *in vivo*. In these circumstances, the numerical Monte Carlo (MC) method is a good solution for simulation of the nanoparticles contrasting effect. Qualitative likeness of the simulated and experimentally obtained OCT images indicates that the effect is provided by nanoparticles, and no significant changes in the skin structure are present. The Monte Carlo method has also been shown to be an effective tool for simulation of OCT signals from multilayer media and evaluation of multiple scattering contri-

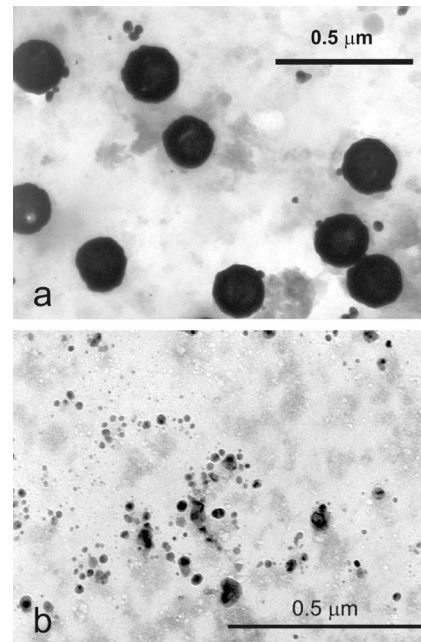


Fig. 1 SEM images of the nanoparticles: (a) gold nanoshells with 75/25 core/shell radii and (b) titanium dioxide nanoparticles.

bution to these signals in our earlier papers.^{29,30} Later, it was advanced for simulation of OCT images from skin phantoms.³¹ Earlier we applied our Monte Carlo technique to study the effect of titanium dioxide nanoparticles on OCT signals,²⁶ and showed that the sizes and concentrations of the nanoparticles present in the upper skin layer dramatically affects the obtained OCT signals. The Monte Carlo simulations were also implemented in Ref. 13 for analysis of effect of silica/gold nanoshells on the diffuse reflectance of biotissue samples.

The aim of the present work is to study the efficiency of silica/gold nanoshells and TiO_2 nanoparticles as contrasting agents in OCT imaging of tissues *in vivo*, and to interpret the obtained experimental images by comparison with Monte Carlo simulations results.

2 Materials and Methods

2.1 Nanoshells and Nanoparticles

In this work, silica/gold nanoshells with a 75-nm silica core radius and 25-nm-thick gold shell characterized by excellent calibration (the deviation from the average size is about 10 nm) were chosen to be endeavored as the contrasting agents for OCT imaging of skin *in vivo* [Fig. 1(a)]. The gold nanoparticles with given parameters exhibit backscattering maximum associated with plasmon resonant in NIR range (850 to 950 nm), which makes them optimal for contrasting of OCT images.³² Silica-gold nanoshells were fabricated as described^{33–35} with minor modifications in the reagent concentrations. First, silica nanoparticles were grown by reducing tetraethyl orthosilicate (Fluka) with NH_4OH in absolute ethanol. Specifically, we added $660\ \mu\text{l}$ of 25% aqua ammonia and $300\ \mu\text{l}$ of tetraethyl orthosilicate (Fluka) to 10 ml of absolute ethanol. Aggregates were removed by filtering the resultant suspension through a nitrocellulose membrane (Milli-

pore, USA) with a mean pore diameter of 0.45 μm .

The second stage involved functionalizing SiO_2 nanoparticles with amine groups by reaction with APTMS in ethanol, as described in Ref. 36. The third stage involved synthesizing gold nanoparticles (“seeds,” 2 to 3 nm in diameter) and attaching them to the silica-core surface.³⁶ The gold colloid adsorbed onto the surfaces of aminated silica as a result of electrostatic interaction. At the final stage, nanoshells were grown by reacting HAuCl_4 with the silica-colloid particles in the presence of formaldehyde at room temperature. This process reduces additional gold on the adsorbed colloid, which acts as nucleation sites. Depending on the ratio between the total particle-surface area of silica and the amount of reduced gold, the resulting nanoshells have differing structures and spectral properties. In this work, nanoshells were designed to have 75-nm core radius and 25-nm shell thickness.

We also used commercially available highly pure (99.999%) titanium dioxide (rutile) by the PROMCHIM Group (Russia). Titanium dioxide nanoparticles were synthesized from a titanium alkoxide process by means of the sol-gel method. Nanoparticles size is 54 ± 12 nm (mean size \pm SD) [Fig. 1(b)]. The motivation for use of this titanium dioxide nanopowder is that it is approved for pharmaceutical and biological applications and has sanitary-epidemiological certification hence it excludes harm to a laboratory animal. Suspended in water, TiO_2 nanoparticles exhibit high levels of aggregation with the average size of aggregates being 400 nm. Suspension was obtained by diluting TiO_2 powder in distilled water in concentration of 10 mg/ml at room temperature, and additional 20-min-long ultrasound impact for avoiding aggregation.

2.2 Test Animals

As the first step in our experiments, the effects of silica/gold nanoshells and titanium dioxide nanoparticles on OCT images after one application on skin were studied. The 25- μl suspension drop was applied *in vivo* on healthy skin areas on the back of a 6-kg pig after depilation. To obtain a reference image, a water drop of the same volume was administered to the neighboring skin area.

The procedure of OCT imaging was chosen based on the experience obtained in previous studies⁸ and optimized with regard to time in a preliminary experiment. At first a reference OCT image was acquired from a native skin site, and second an OCT image was obtained immediately on application of the chemical agent. Subsequent images were taken for both types of contrasting agents every 30 min during 5 h and then after 24 h. Identification of skin layers on the OCT images was made by comparing the histology sample images. Samples for light microscopy were obtained by a standard method of staining with hematoxylin and eosin. The biopsy of the corresponding skin samples for electron microscopy was performed 3 and 24 h after nanoparticles application.

2.3 Optical Coherence Tomography System

The OCT system produced by the Institute of Applied Physics of RAS (Nizhny Novgorod, Russia) equipped with a flexible probe was applied in the present study.³⁷ The system has the following characteristics: outer diameter of the probe is 2.7 mm, probing wavelength is 900 nm, power of the probing

radiation is 2 mW, spatial resolution in air is about 15 μm , and the average time for obtaining a 2-D image of 200×200 pixels is 1.5 sec. The OCT probe was positioned on the skin surface perpendicularly with the uniform pressure distribution over the area under study.³⁸

2.4 Monte Carlo Simulation of Optical Coherence Tomography Images

The Monte Carlo (MC) simulation method is based on calculating a large numbers of the trajectories of photons randomly propagating in a scattering medium.³⁹ The optical properties of the medium (scattering and absorption coefficients, phase function or anisotropy factor, and refractive index) determine the lengths and shapes of individual photon trajectories. We used a program code of the MC algorithm developed earlier²⁹⁻³¹ for simulation of the OCT signals and images. In the simulation, we used the Henyey-Greenstein phase function, which is widely used for MC simulations of light propagation in biotissues, including skin:⁴⁰

$$f_{\text{HG}}(\theta) = \frac{1}{4\pi} \frac{(1-g^2)}{[1+g^2-2g\cos(\theta)]^{3/2}}, \quad (1)$$

where θ is the scattering angle, and g is the anisotropy factor.

To simulate the 2-D OCT image, the consequent OCT A-scans are simulated with the definite step in the probing position. The total number of A-scans and the step between them are predefined. The step is usually chosen as a width [full width at half maximum (FWHM)] of the probing beam diameter.

For simulating the OCT images of a multilayer skin phantom, we considered the experimental OCT setup in which $\lambda = 910$ nm and coherence length $l_{\text{coh}} = 10$ μm . For calculating a 2-D OCT image, 50 A-scans with a transversal step of 20 μm were obtained. The typical calculation of an OCT image of skin took about 10 h at a PC with an AMD Athlon™ 3000 processor.

2.5 Effect of Nanoparticles on Optical Properties of Skin

In Ref. 13, the authors stated that the adding of nanoshells does not affect significantly the anisotropy factor of the media, arguing that the volume fraction of the nanoshells inside the medium is negligibly small. However, in our opinion the scattering cross sections should be taken into account instead of physical size in such an evaluation. The proposed model allows one to account this point accurately. Unlike Ref. 26, where the effective phase function was calculated as a sum of skin phase function and nanoparticles phase function with a given weight depending on the concentration of nanoparticles, we used a different approach. The presence of nanoparticles in the skin layer was accounted for in the MC simulations by defining the probabilities for a photon to scatter on a skin scattering element, or a nanoparticle based on the preset concentration of the nanoparticles in the layer. The optical characteristics of a single nanoparticle such as scattering and absorption efficiencies Q_s and Q_a , together with scattering phase function for nonpolarized light, were calculated implementing the Mie theory for uniform spheres, or for spheres with coating for cases of TiO_2 and gold nanoshells correspondingly using the values for complex refractive index of the com-

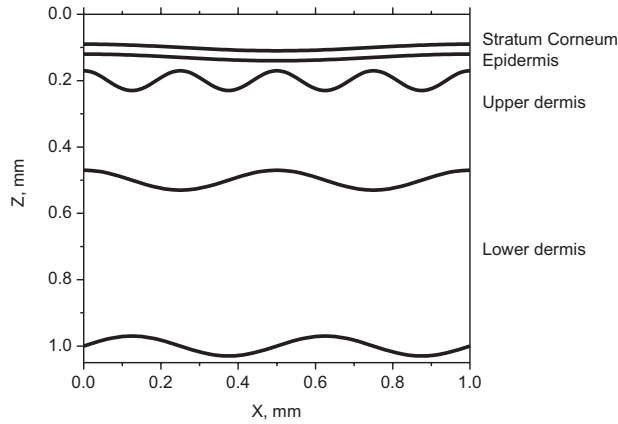


Fig. 2 Four-layer thin skin model used in the Monte Carlo simulations.

pound materials. The general Mie solution for coated spheres was shown in Ref. 41 For calculations, Mätzler's MATLAB codes were used.⁴² The scattering and absorption cross sections were obtained from the corresponding efficiencies using the formulae:

$$\sigma_s = \frac{Q_s}{\pi r^2}, \quad \sigma_a = \frac{Q_a}{\pi r^2},$$

where r is the radius of the considered nanoparticle. The partial scattering and absorption coefficients introduced by the presence of the nanoparticles were calculated according to the formula:

$$\mu_s^{\text{np}} = \sigma_s C, \quad \mu_a^{\text{np}} = \sigma_a C,$$

where C is the concentration of nanoparticles in the skin layer. Resulting scattering and absorption coefficients of the skin layer with embedded nanoparticles were calculated as follows:

$$\mu_s = \mu_s^{\text{np}} + \mu_s^{\text{skin}}, \quad \mu_a = \mu_a^{\text{np}} + \mu_a^{\text{skin}},$$

where μ_s^{skin} , μ_a^{skin} are the scattering and absorption coefficients of the skin layer without nanoparticles.

The resulting anisotropy factor g can be calculated as

$$g = \frac{\mu_s^{\text{skin}} g^{\text{skin}} + \mu_s^{\text{np}} g^{\text{bp}}}{\mu_s^{\text{skin}} + \mu_s^{\text{np}}}. \quad (2)$$

2.6 Multilayer Model of Skin

The four-layer skin models based on the experimental images were utilized in the simulation; the schematic of this model is shown in Fig. 2. The optical properties values used in the simulations are presented in Table 1. Because the pig skin is close to human in its optical properties, these values are obtained by averaging the values obtained for human skin in Refs. 40 and 43. The skin layers were supposed to be characterized by the Henyey-Greenstein phase function, while the scattering phase function of the nanoparticles embedded into skin was calculated using the Mie theory.^{44,45} The layers are supposed to contain uniformly distributed nanoparticles or not contain them at all. Because in the experiment it was impossible to evaluate the concentration of the particles, the concentration of the particles in the simulations was varied in the range, providing the contrasting effect.

A spherical hair bulb of 0.05 mm radius was considered present in the upper dermis at the physical depth of 0.15 mm from the top of the sample to study the contrasting of such elements within skin.

The aim of MC simulations is to prove that the contrasting effect observed in the experiment originates from the presence of nanoparticles, not due to other changes in skin properties caused by their application. To reach this goal, only the effect of nanoparticles was taken into account in the simulations; the effect of optical clearing caused by particle solvents as well as changes in skin structure caused by the application were not considered.

2.7 Optical Properties of Nanoparticles

In simulations we consider two types of nanoparticles corresponding to the ones used in the experiment: gold nanoshells with silica core of 75 nm radius and gold coating with thickness of 25 nm, and TiO₂ nanoparticles with radius of 50 nm. The values of complex refractive index for silica, gold, and TiO₂ at a wavelength of 820 nm used for the calculations are as follows:^{46,47}

$$n_{\text{SiO}_2} = 1.4524 + i0.005,$$

$$n_{\text{Au}} = 0.17 + i5.663,$$

$$n_{\text{TiO}_2} = 2.59 + i0.005.$$

The optical properties of the nanoparticles calculated with the Mie theory are presented in Table 2. The concentrations of the

Table 1 Optical properties of skin layers ($\lambda=900$ nm).

Number	Skin layer	Thickness (mm)	μ_s (mm ⁻¹)	μ_a (mm ⁻¹)	g	n
1	Stratum corneum	0.03	35	0.02	0.9	1.45
2	Epidermis	0.07	12	0.1	0.9	1.39
3	Upper dermis	0.3	7	0.7	0.85	1.4
4	Lower dermis	0.5	12	0.1	0.9	1.4

Table 2 Optical properties of nanoparticles and nanoshells.

Particle type	r (nm)	σ_s (μm^2)	σ_a (μm^2)	g
SiO ₂ /Au	75/25	0.133	0.0072	-0.027
TiO ₂	50	$2.47 \cdot 10^{-4}$	$2.40 \cdot 10^{-5}$	0.053

nanoparticles varied from 0.001 to 0.01 volume % for SiO₂/Au nanoshells and from 0.01 to 0.5 volume % for TiO₂ nanoparticles (for SiO₂/Au particles 1 volume % = $2.4 \cdot 10^9$ particles/ml, and for TiO₂ particles 1 volume % = $1.9 \cdot 10^{10}$ particles/ml). The corresponding values for μ_s^{np} vary from 0.320 to 3.20 mm⁻¹ for SiO₂/Au nanoshells, and from 0.047 to 2.36 mm⁻¹ for TiO₂ nanoparticles. The corresponding values for μ_a^{np} vary from 0.0172 to 0.172 mm⁻¹ for SiO₂/Au nanoshells, and from 0.0046 to 0.230 mm⁻¹ for TiO₂ nanoparticles.

The scattering phase functions of a single particle both for TiO₂ and SiO₂/Au nanoparticles compared to that of skin layers considered in the present study are presented in Fig. 3. From this figure one can see that skin is characterized by strongly forward-elongated phase functions, while nanoparticles exhibit backscattering maxima that provide an increase in the amount of backscattering photons at the presence of these particles in the skin sample, and hence, an increase in the contribution to the OCT image.

With Eq. (2), one can evaluate the change in the anisotropy factor induced by the presence of nanoparticles. For example, the anisotropy factor of upper dermis changes from 0.85 to 0.812 or 0.575 when SiO₂/Au nanoshells with concentrations of 0.001 or 0.01 volume % correspondingly are added. TiO₂ nanoparticles with concentrations of 0.01 or 0.5 volume % change the upper dermis anisotropy factor to 0.845 or 0.649 correspondingly.

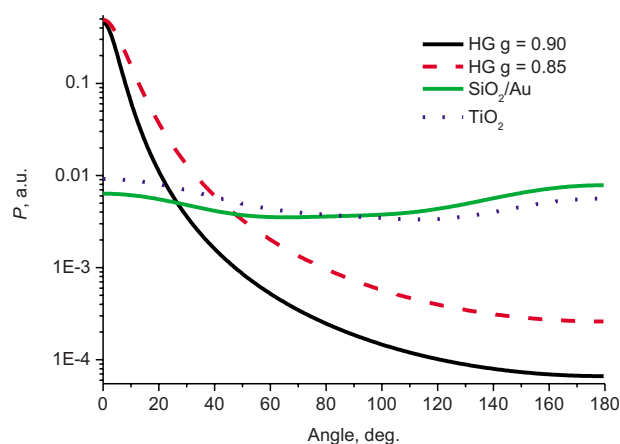


Fig. 3 Scattering phase functions of TiO₂ (50 nm radius) and SiO₂/Au (75/25-nm core/coating radius) nanoparticles and Henyey-Greenstein (HG) phase function for $g=0.85$ and 0.9 characterizing skin layers.

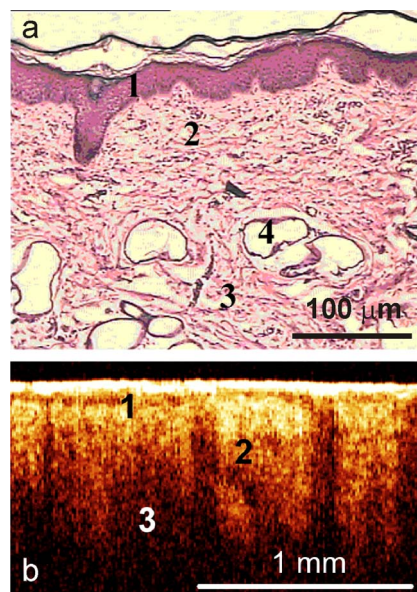


Fig. 4 (a) Histology image and (b) OCT image of pig skin before silica/gold nanoshells application: 1 epidermis, 2 superficial part of the dermis, 3 deep layers of the dermis, and 4 glands. Histology slice was stained by hematoxylin-eosin.

3 Results

3.1 Reference Optical Coherence Tomography Images without Contrast Agents

Comparison of a typical OCT image with histological images shows that it is difficult to distinguish separate layers and structures in the OCT images of pig skin obtained without any contrasting agents (Fig. 4). The upper layer characterized by high brightness corresponds to the area where the surface of the OCT probe is adjacent to the pig skin surface. A thin darker layer corresponds to the epidermis in the histology image (the thickness is 0.07 mm on average). Under the epidermis there lies derma. We can distinguish in the histology image the upper (0.3 mm) and the lower (0.5 mm) dermis. The upper dermis contains hair follicles and glandular ducts, and the lower dermis contains glands. These layers are indistinguishable in the OCT image; they look like an inhomogeneous region with an average or low signal level. We further identify them by inclusions typical for these layers. Inclusions are not encountered in OCT images without additional contrasting.

3.2 Optical Coherence Tomography Effects of Gold Nanoshells and Nanoparticles of Titanium Dioxide on Skin In Vivo

A single application of gold nanoshells on skin surface induces a number of alterations of OCT images. The epidermis becomes uniform, homogeneous, and has a distinct border with the underlying dermis [Figs. 5(b) and 5(c)]. Signal intensity in the upper dermis increases [Fig. 5(b)]. Inclusions characterized as low signal intensity areas appear. These are small, round, or slightly elongated inclusions with well-defined contours in the upper derma [Fig. 5(c)] and/or large, diagonally oriented inclusions with poorly defined contours [Fig. 5(b)].

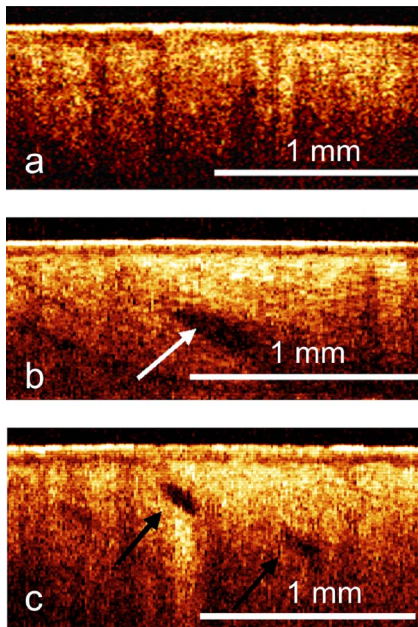


Fig. 5 OCT images of pig skin at application of gold nanoparticles: (a) reference without particles, (b) 90 min, and (c) 150 min. The arrows indicate inclusions recognized as a hair follicle [in (b)] and glandular ducts [in (c)].

At a single application of titanium dioxide nanoparticles on skin surface, the observed effects were analogous to those with gold nanoparticles. We detected contrast of the border between the epidermis and upper dermis, increase of signal intensity in the upper dermis, and visualized inclusions in the upper derma [Fig. 6(b)]. But, in addition to the effects de-

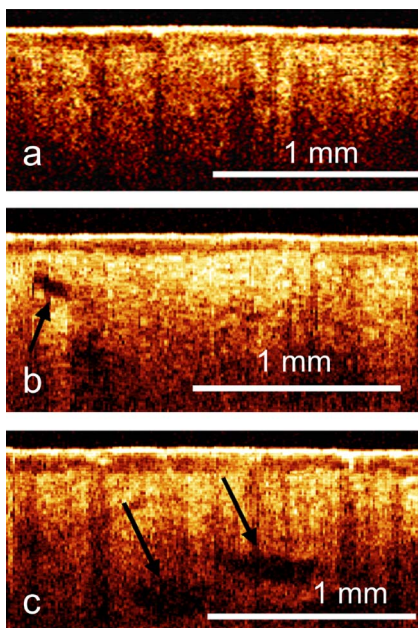


Fig. 6 OCT images of pig skin at application of titanium dioxide nanoparticles: (a) control without particles, (b) 60 min, and (c) 180 min. The arrows indicate inclusions recognized as a glandular duct [in (b)] and glands [in (c)].

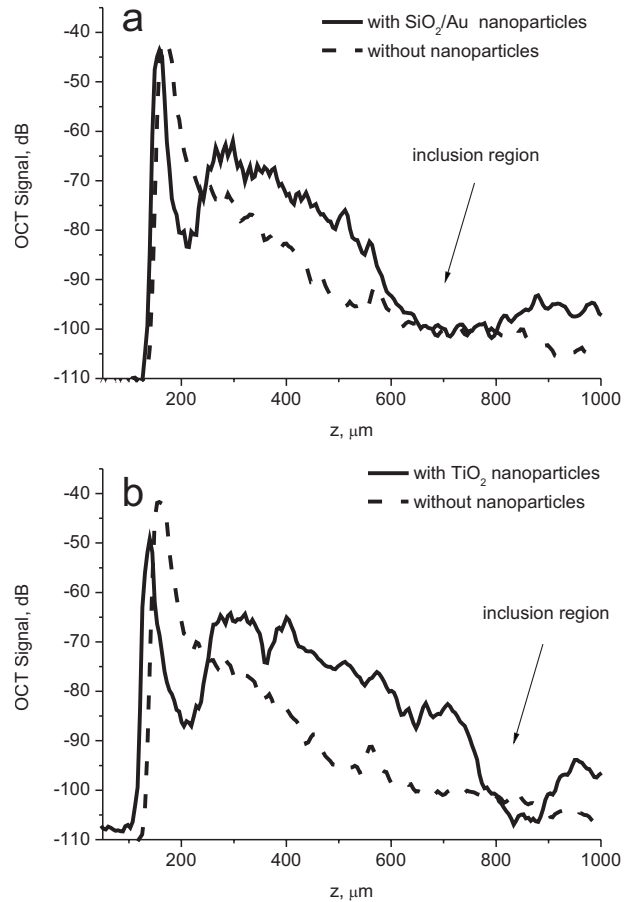


Fig. 7 OCT A-scans of pig skin for maximum efficiency of contrasting agents: (a) silica/gold nanoparticles, and (b) TiO_2 nanoparticles. The dash line shows averaged A-scans of the reference image (prior to application of agents).

scribed before, in the lower derma low signal-intensity inclusions with oval shape and well-defined contours appear [Fig. 6(c)].

Analysis of the A-scans (Fig. 7) confirms the observed effects for both cases: application of gold nanoparticles and titanium dioxide nanoparticles. The contrast of the border of the epidermis is represented by the drop of signal intensity and is approximately the same for both types of nanoparticles. One can see in the plots the signal increase in the upper derma. Both types of the particles contrasted inclusions in the dermis, which are represented by the signal jump at their border (as shown by arrows). The signal level is different for contrasting different types of inclusions: in the case of oval inclusions contrasted by titanium oxide, the signal drop in the lower dermis is more pronounced than in the case of diagonally oriented inclusions in the upper dermis when gold nanoshells are employed. Comparison of different types of inclusions in images with the corresponding histology slides enables us to conjecture that round and diagonal inclusions in the upper dermis are, respectively, glandular ducts and hair follicles, whereas oval inclusions in the lower derma are glands. The reference group featured uniform signal decay in depths without pronounced jumps.

Table 3 Typical times of contrasting effects induced in OCT images of skin by SiO₂/Au and TiO₂ nanoparticles

Contrasting effect	SiO ₂ /Au	TiO ₂
Contrasting of epidermis-dermis border	0.5 to 24 h	1 to 24 h
Contrasting of inclusions in upper dermis	1 to 2.5 h	2 to 24 h
Contrasting of inclusions in lower dermis	2 to 4 h	3.5 to 24 h
Dark stripes artifacts	–	0–1 h

The typical times of the effects of gold nanoshells and TiO₂ nanoparticles on OCT images are presented in Table 3. According to our observations, gold nanoshells are characterized by early manifestation of the contrasting effects, which does not last long, whereas in the case of titanium dioxide the effects appear later but last longer.

The presence in skin samples of the studied contrasting agents was confirmed by electron microscopy (Fig. 8). Three hours after application, nanoparticles are rarely encountered in the epidermis. They are detected primarily in dermis: in fibroblasts and among collagen fibers, inside cells, and in intercellular substance. In 24 h, there are fewer nanoparticles in skin: they are encountered primarily in dermis, both in the upper and in deep layers. The amount of gold nanoshells detected in skin is smaller than that of titanium dioxide particles.

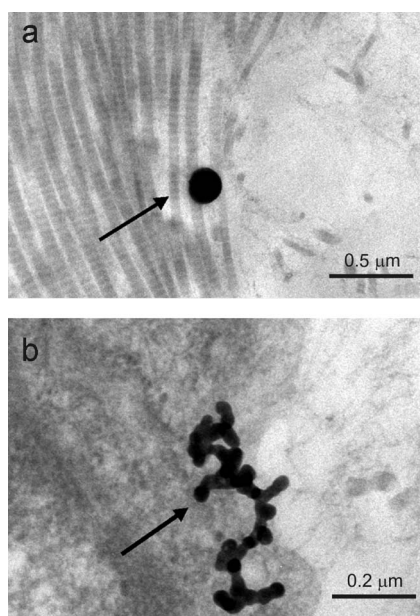


Fig. 8 Electron micrography of pig skin 24 h after application of gold nanoshells and TiO₂ nanoparticles: (a) gold nanoparticles in dermis among collagen fibers, and (b) aggregated TiO₂ nanoparticles in epidermis. The arrows indicate nanoparticles.

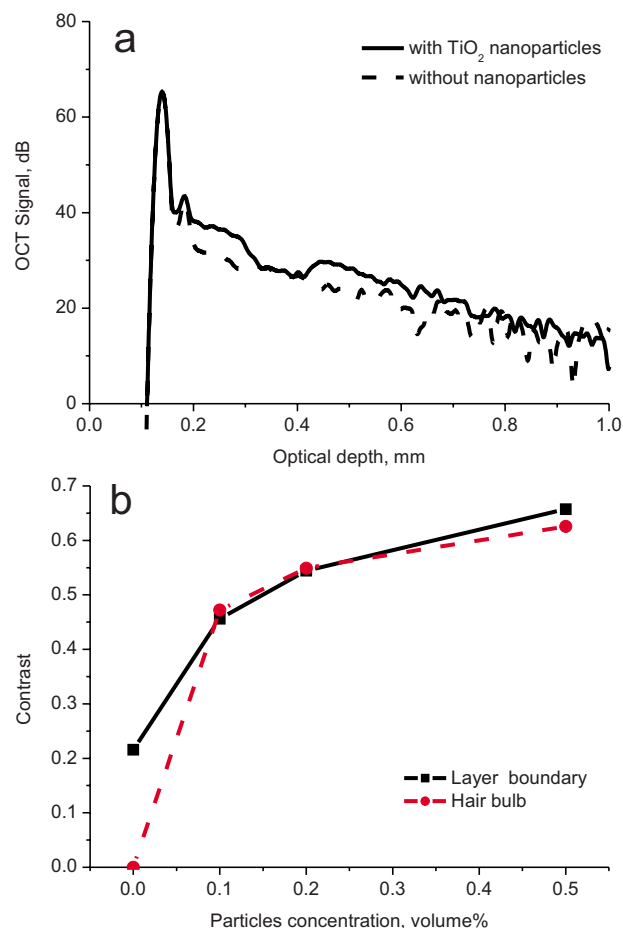


Fig. 9 (a) Simulated OCT A-scans of pig skin before and after application of TiO₂ nanoparticles (concentration of the nanoparticles is 0.5 volume %) (b) and corresponding contrast of the image elements for various concentrations.

3.5 Monte Carlo Simulation Results

When performing MC simulations, we supposed that the nanoparticles penetrate only two or three upper layers of the considered skin model—stratum corneum, epidermis, and upper dermis. The border between upper and lower dermis was supposed to have a wavy shape, and its contrast was chosen as a criterion for effectiveness of the nanoparticles application.

At first the OCT A-scans from the pig skin were calculated for various concentrations of nanoparticles for both particle types to quantitatively evaluate the contrasting effect of the nanoparticles' presence. The results for TiO₂ nanoparticles are shown in Fig. 9. The OCT scans are shown for the case when particles are present in the upper two layers. From this figure one can see that application of the nanoparticles significantly increases the contrast of the epidermis-dermis border [Fig. 9(a)]. Figure 9(b) depicts quantitative evaluation of the contrast increase. The contrast of the layer border and hair bulb is evaluated when nanoparticles are present in the two and three upper layers of the skin sample correspondingly.

Similar results for SiO₂/Au particles are presented in Fig. 10. From this figure one can see that these particles provide an increase in contrast compared to TiO₂ particles, although the concentration is significantly lower. This fact is explained by

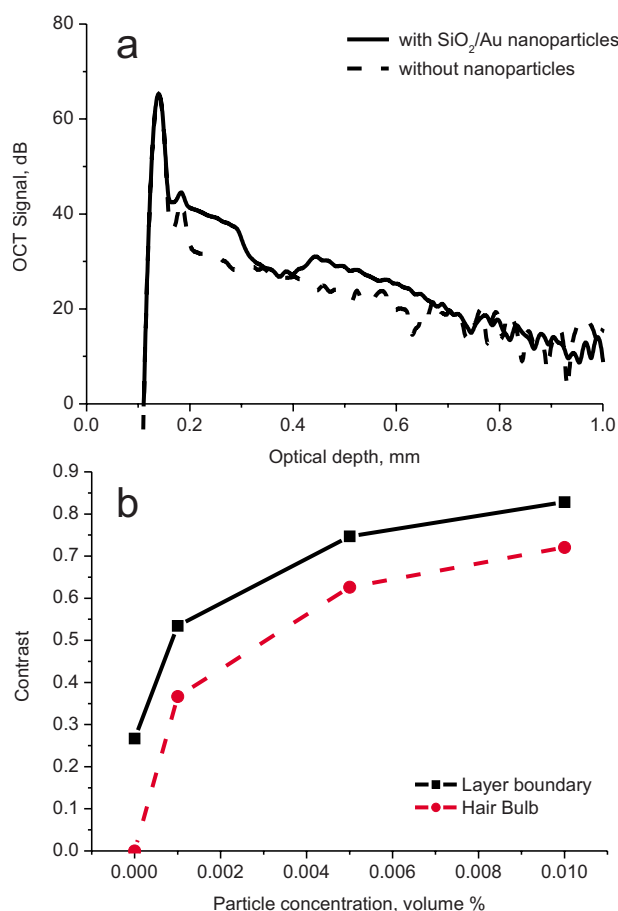


Fig. 10 (a) Simulated OCT A-scans of pig skin before and after application of SiO_2/Au nanoparticles (concentration of the nanoparticles is 0.01 volume %) (b) and corresponding contrast of the image elements for various concentrations.

a significantly larger scattering cross section of SiO_2/Au particles compared to TiO_2 ones (see Table 2).

At the next stage, the OCT images were simulated to show the qualitative effect of the nanoparticles. The results of the simulations show that in the absence of the nanoparticles in the model skin sample, the border between the two dermis layers is not contrasted (Fig. 11), while when considering the presence of nanoparticles in the two upper layers, the border becomes contrasted [Figs. 12(a) and 13(a)] for both types of nanoparticles. However, the SiO_2/Au nanoshells provide better contrast, although the concentration of the particles is much lower. The intensity of the OCT signal from the upper layers increases due to increase in backscattering from these areas caused by the presence of the nanoparticles, while the intensity of the signal from the deeper layer remains the same.

Figures 12(b) and 13(b) depict the OCT image of the pig skin sample in the presence of Si/Au and TiO_2 nanoparticles in the three upper layers correspondingly. From these figures one can see that the contrast effect in this case is higher for SiO_2/Au nanoparticles as well.

Thus, Monte Carlo simulation proves that the presence of both SiO_2/Au and TiO_2 nanoparticles introduces an increase in contrast of the inclusions in the OCT images. The effect of

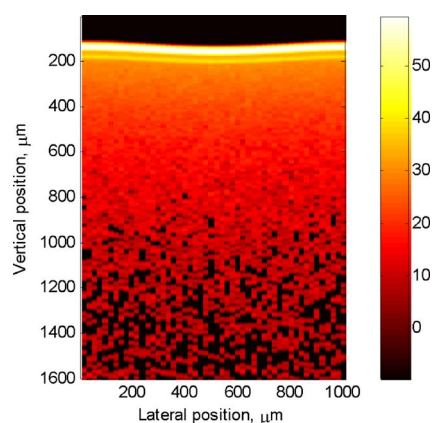


Fig. 11 Simulated OCT image of skin before application of the nanoparticles (reference image).

SiO_2/Au is higher due to their higher scattering cross sections compared to TiO_2 nanoparticles.

4 Discussion and Conclusions

We studied the possibility of surface application of gold nanoshells of 75/25-nm silica/gold radii and titanium dioxide nanoparticles of 54 nm radius for contrasting OCT images of healthy pig skin.

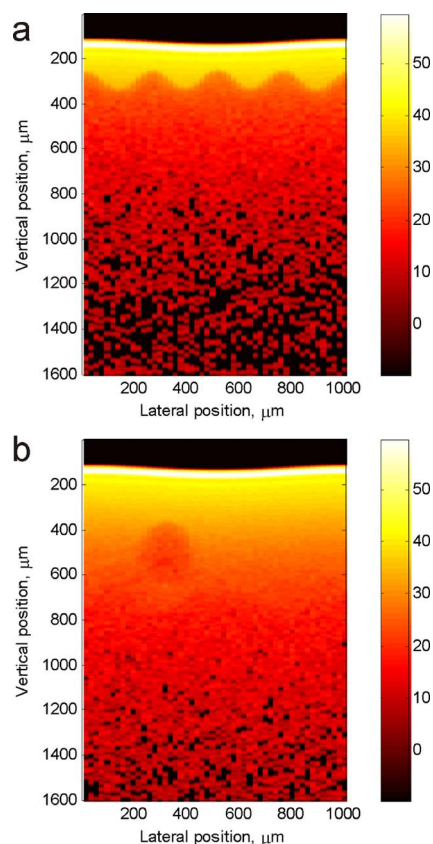


Fig. 12 Simulated OCT images of skin in presence of SiO_2/Au nanoshells in (a) two upper layers and (b) three upper layers. The concentration of the nanoparticles is 0.01 volume %.

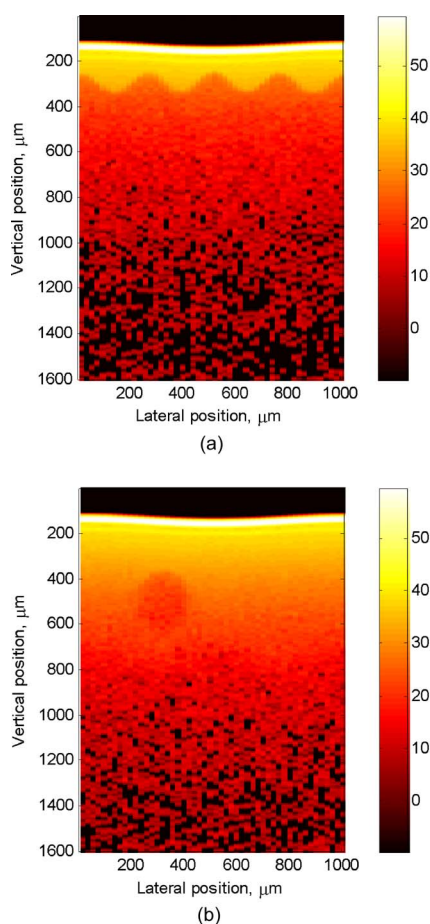


Fig. 13 Simulated OCT images of skin in the presence of TiO_2 nanoparticles in (a) two upper layers and (b) three upper layers. The concentration of the nanoparticles is 0.5 volume %.

In the presented research, the object of contrast is skin characterized by a complex layer structure and the presence of inclusions; the nanoparticle suspension is applied to its surface. We found that nanoparticles rapidly and efficiently penetrate into intact skin, and demonstrated that gold nanoshells have a contrasting effect on skin structures. The duration of optical effects is similar to the case of intravenous injection.²⁰ Maximum contrasted images were obtained in 2 to 4 h; the effects persisted up to 24 h (Table 3). Therefore, local applications of nanoparticles may be quite efficient for contrasting skin structures.

In our study, aqueous suspension of particles rather than an oil-in-water emulsion was applied to skin. Evidently, the properties of particles, including their penetrability into skin, may depend on whether they are in aqueous suspension or in an oil-in-water emulsion. We used the electron microscopy method to confirm that both gold nanoshells and titanium dioxide nanoparticles penetrated into all skin layers and structures. They could penetrate there through intracellular space, cells, or skin appendages (hair follicles, and sebaceous and sweat glands).²⁸

Comparison of the optical effects of gold nanoshells and titanium dioxide nanoparticles by the OCT technique revealed common contrasting effects, as well as particular differences.

Both gold nanoshells and TiO_2 nanoparticles provided contrast of the epidermis layer, which lasted the entire time of observation (24 h). The gold nanoshells provided the contrast of inclusions in the upper dermis layer, which were observed at their best 2 to 4 h after the application following weakening of the effect. The TiO_2 nanoparticles provided visualization of inclusions both in upper and lower dermis layers, which became strongest 3.5 h after application and lasted for 24 h. Possibly the difference in the effects is stipulated by a different chemical nature and different optical properties. Gold nanoshells are heterogeneous nanoparticles capable of generating surface plasmon resonance, whereas titanium dioxide nanoparticles exhibit only a high backscattering coefficient. Gold nanoshells do not aggregate and penetrate into skin faster; therefore, the effects arise earlier. Titanium dioxide nanoparticles form aggregates on the surface of the skin, which slow down particle penetration significantly. We believe that the ability of titanium dioxide nanoparticles to contrast deep inclusions indicates that they penetrate deeper into skin than gold nanoshells. Perhaps enhanced permeation of titanium particles is bound to the fact that the polydisperse titanium particles include many particles that are significantly smaller than the diameter of the gold core-shell nanoparticles used. Moreover, the concentration of gold nanoparticles in solution is 500 times less compared to the concentration of titanium dioxide nanoparticles, hence they are distributed primarily in the upper skin layers.

The contrasting effect of nanoparticles was also confirmed by Monte Carlo simulations. The simulations were performed both for titanium dioxide nanoparticles and gold nanoshells. In the model, the only change in scattering properties introduced by the particles was taken into account. In both cases the results demonstrate the contrasting effect manifested by contrast of the epidermis-dermis border for the case when the particles penetrate only in epidermis, and the contrast of spherical inclusion in dermis, when the particles penetrate deeper. These facts allow us to conclude that the exhibited effect originates from the presence of nanoparticles in skin, not from accompanying effects induced by the presence of the particles. The numerical results also shown that for gold nanoshells, significantly smaller concentrations compared to that of titanium dioxide are needed to provide a contrasting effect. This fact agrees with the experimental results and originates from much larger scattering cross sections of gold-nanoshells and their backscattering maxima caused by plasmon resonance.

Thus, one can conclude that both gold nanoshells and TiO_2 nanoparticles can serve as efficient contrasting agents in visualization of *in vivo* skin by OCT. The gold nanoparticles are characterized by plasmon resonance, providing stronger backscattering compared to TiO_2 nanoparticles, which require much smaller concentrations of gold nanoshells for providing the contrast effect. On the other hand, TiO_2 nanoparticles exhibited larger contrast depth and longer contrast effects.

Acknowledgments

This work was partly supported by the Science and Innovations Federal Russian Agency (project numbers 02.522.11.2004 and 02.512.11.2244), and the Russian Foundation for Basic Research (grant numbers 09-02-00354 and

09-02-00539). The authors are grateful to L.B. Snopova (Nizhny Novgorod State Medical Academy) for help in performance of the microscopic analysis procedure. Also the authors thank the Institute of Biochemistry and Physiology of Plants and Microorganisms (Saratov, Russia), and companies in the PROMCHIM Group (Russia) for providing nanoparticles.

References

- J. M. Fujimoto, C. Pitris, S. A. Boppart, and M. E. Brezinski, "Optical coherence tomography, an emerging technology for biomedical imaging, and optical biopsy," *Neoplasia* **2**, 9–25 (2000).
- A. M. Sergeev, V. M. Gelikonov, G. V. Gelikonov, F. I. Feldchtein, R. V. Kuranov, N. D. Gladkova, N. M. Shakhova, L. B. Snopova, A. V. Shakhov, I. A. Kuznetsova, A. N. Denis-enko, V. V. Pochinko, Y. P. Chumakov, and O. S. Streltsova, "In vivo endoscopic OCT imaging of precancer and cancer states of human mucosa," *Opt. Express* **1**, 432–440 (1997).
- A. M. Sergeev, L. S. Dolin, and D. N. Reitze, "Optical tomography of biotissues past, present, and future," *Opt. Photonics News* **12**, 28–35 (2001).
- F. I. Feldchtein, N. D. Gladkova, L. B. Snopova, E. V. Zagaynova, O. S. Streltsova, A. V. Shakhov, A. V. Terentjeva, N. M. Shakhova, I. A. Kuznetsova, G. V. Gelikonov, V. M. Gelikonov, V. A. Kamensky, and V. A. Danchenko, "Coherence domain optical methods in biomedical science, and clinical application," *Proc. SPIE* **4956**, 89–94 (2003).
- E. V. Zagaynova, M. V. Shirmanova, A. G. Orlova, I. V. Balalaeva, M. Yu. Kirillin, and V. A. Kamensky, "In vivo study of contrasting properties of gold nanoshells for optical coherence tomography," *Proc. SPIE* **6633**, 663316 (2007).
- A. G. Petrova, E. N. Derpalyuk, N. D. Gladkova, N. K. Nikulin, R. R. Iksanov, V. M. Gelikonov, G. V. Gelikonov, and E. V. Donchenko, "Ways of increase of OCT informativity in dermatocosmetology," *Exper. Clin. Dermatocosmet.* **3**, 10–17 (2005) [in Russian].
- S. G. Proskurin and I. V. Meglinski, "Optical coherence tomography imaging depth enhancement by superficial skin optical clearing," *Laser Phys. Lett.* **4**, 824–826 (2007).
- R. K. Wang and J. B. Elder, "Propylene glycol as a contrasting agent for optical coherence tomography to image gastrointestinal tissue," *Lasers Surg. Med.* **30**, 201–208 (2002).
- V. V. Tuchin, *Optical Clearing of Tissues, and Blood*, SPIE Press, Bellingham, WA (2006).
- V. V. Tuchin, "Optical clearing of tissues, and blood using the immersion method," *J. Phys. D: Appl. Phys.* **38**, 2497–2518 (2005).
- G. F. Paciotti, L. Myer, D. G. I. Kingston, T. Ganesh, and L. Tamarkin, "A verticale platform for developing tumor targeted cancer therapies," in *Tech. Proc. of the 2005 NSTI Nanotechnology Conference and Trade Show*, vol. 1, pp. 7–10, NSTI (2005).
- V. Zharov, R. R. Letfullin, and E. N. Galitovskaya, "Microbubbles-overlapping mode for laser killing of cancer cell with absorbing nanoparticles clusters," *J. Phys. D: Appl. Phys.* **38**, 2571–2585 (2005).
- A. W. H. Lin, N. A. Lewinski, J. L. West, N. J. Halas, and R. A. Drezek, "Optical tunable nanoparticle contrast agents for early cancer detection: model-based analysis of gold nanoshells," *J. Biomed. Opt.* **10**, 064035 (2005).
- A. L. Oldenburg, M. N. Hansen, D. A. Zweifel, A. Wei, and S. A. Boppart, "Plasmon-resonant gold nanorods as low backscattering albedo contrast agent for optical coherence tomography," *Opt. Express* **14**(15), 6724–6738 (2006).
- H. Cang, T. Sun, Z. Y. Li, J. Chen, B. J. Wiley, and Y. Xia, "Gold nanocages as contrast agent for spectroscopic optical coherence tomography," *Opt. Lett.* **30**(22), 3048–3050 (2005).
- Y. Xia and N. J. Halas, "Shape-controlled synthesis, and surface plasmonic properties of metallic nanostructures," *MRS Bull.* **30**(5), 338–348 (2005).
- C. Loo, A. Lin, L. Hirsch, M. H. Lee, J. Barton, N. Halas, J. West, and R. Drezek, "Nanoshell-enabled photonics-based imaging, and therapy of cancer," *Technol. Cancer Res. Treat.* **3**(1), 33–40 (2004).
- B. Khlebtsov, V. Zarov, A. Melnikov, V. Tuchin, and N. Khlebtsov, "Optical amplification of photothermal therapy with gold nanoparticles, and nanoclusters," *Nanotechnology* **17**, 5167–5179 (2006).
- T. M. Lee, A. L. Oldenburg, S. Sitafalwalla, D. L. Marks, W. Luo, F. J. J. Toublan, K. S. Suslick, and S. A. Boppart, "Engineered microsphere contrast agents for optical coherence tomography," *Opt. Lett.* **28**, 1546–1548 (2003).
- A. M. Gobin, M. H. Lee, N. J. Halas, W. D. James, R. A. Drezek, and J. L. West, "Near infrared resonant nanoshells for combined optical imaging, and photothermal cancer therapy," *Nano Lett.* **7**, 1929–1934 (2007).
- E. V. Zagaynova, M. V. Shirmanova, M. Yu. Kirillin, B. N. Khlebtsov, A. G. Orlova, I. V. Balalaeva, M. A. Sirotkina, M. L. Bugrova, P. D. Agrba, and V. A. Kamensky, "Contrasting properties of gold nanoparticles for optical coherence tomography: phantom, in vivo studies, and Monte Carlo simulation," *Phys. Med. Biol.* **53**, 4995–5009 (2008).
- R. F. Edlich, K. L. Winter, H. W. Lim, M. J. Cox, D. J. Becker, J. H. Horovitz, L. S. Nichter, L. D. Britt, and W. B. Long, "Photoprotection by sunscreens with topical antioxidants systemic antioxidants to reduce sun exposure," *Long-Term Effects Med. Implants* **14**(4), 317–340 (2004).
- B. Innes, T. Tsuzuki, H. Dawkins, J. Dunlop, G. Trotter, M. R. Nearn, P. G. McCormick, and F. Edlich, "Nanotechnology, and the cosmetic chemist," *Cosmet. Aero. Toilet. Australia* **15**(10–12), 21–24 (2002).
- J. Lademann, H. J. Weighmann, H. Schaefer, G. Muller, and W. Sterry, "Investigation of the stability of coated titanium microparticles used in sunscreens," *Skin Pharmacol. Appl. Skin Physiol.* **13**, 258–264 (2000).
- A. Agrawal, S. Huang, A. W. H. Lin, M. H. Lee, J. K. Barton, R. A. Drezek, and T. J. Pfefer, "Quantitative evolution of optical coherence tomography signal enhancement with gold nanoshells," *J. Biomed. Opt.* **11**, 041121 (2006).
- A. P. Popov, M. Y. Kirillin, A. V. Priezzhev, J. Lademann, J. Hast, and R. Myllyla, "Optical sensing of titanium dioxide nanoparticles within horny layer of human skin, and their protecting effect against solar UV radiation," *Proc. SPIE* **5702**, 113–122 (2005).
- J. Schulz, H. Hohenberg, F. Pfluger, E. Gartner, T. Will, S. Pfeiffer, R. Wepf, V. Wendel, H. Gers-Barlag, and K. P. Wittem, "Distribution of sunscreens on skin," *Adv. Drug Delivery Rev.* **54**, 157–163 (2002).
- P. J. A. Borm, D. Robbins, S. Haubold, T. Kuhlbusch, H. Fissan, K. Donaldson, R. Schins, V. Kreyling, J. Lademann, J. Krutmann, D. Warheit, and E. Oberboster, "The potential risk of nanomaterials: a review carried out for ECETOC," *Part Fibre Toxicol.* **3**, 11–23 (2006).
- M. Yu. Kirillin, I. V. Meglinskii, and A. V. Priezzhev, "Effect of photons of different scattering orders on the formation of a signal in optical low-coherence tomography of highly scattering media," *Quantum Electron.* **36**, 247–252 (2006).
- M. Yu. Kirillin, A. V. Priezzhev, V. V. Tuchin, R. K. Wang, and R. Myllyla, "Effect of red blood cell aggregation, and sedimentation on optical coherence tomography signals from blood samples," *J. Phys. D: Appl. Phys.* **38**, 2582–2589 (2005).
- I. Meglinski, M. Kirillin, V. Kuzmin, and R. Myllyla, "Simulation of polarization-sensitive optical coherence tomography images by Monte Carlo method," *Opt. Lett.* **33**(14), 1581–1583 (2008).
- L. A. Trachuk, S. A. Vrublevsky, B. N. Khlebtsov, A. G. Melnicov, N. G. Khlebtsov, and D. A. Zimnyakov, "Optical properties of gold spheroidal particles, and nanoshells: effect of the external dielectric medium," *Proc. SPIE* **5772**, 1–10 (2005).
- C. Loo, M.-H. Lee, L. Hirsch, E. Chang, J. West, N. Halas, and R. Drezek, "Gold nanoshell bioconjugates for molecular imaging in living cells," *Opt. Lett.* **30**, 1012–1014 (2005).
- S. J. Oldenburg, R. D. Averitt, S. L. Westcott, and N. Halas, "Nanoeengineering of optical resonances," *Chem. Phys. Lett.* **288**, 243–247 (1998).
- T. Pham, J. B. Jackson, N. J. Halas, and T. R. Lee, "Preparation, and characterization of gold nanoshells coated with self-assembled monolayers," *Langmuir* **18**, 4915–4920 (2002).
- B. N. Khlebtsov, V. A. Bogatyrev, L. A. Dykman, and N. G. Khlebtsov, "Spectra of resonance light scattering of gold nanoshells: effects of polydispersity, and limited electron free/path," *Opt. Spectrosc.* **102**, 233–238 (2007).
- V. M. Gelikonov, G. V. Gelikonov, L. S. Dolin, V. A. Kamensky, A. M. Sergeev, N. M. Shakhova, N. D. Gladkova, and E. V. Zagaynova, "Optical coherence tomography: physical principles, and applications," *Laser Phys.* **13**(5), 692–702 (2003).
- V. V. Vorobiev, G. V. Gelikonov, V. M. Gelikonov, V. A. Kamensky, M. B. Prudnikov, and I. V. Turchin, "Device for obtaining contrasted

- OCT images,” claim for patent 2006103448 from 06.02.2006 (in Russian).
39. L. Wang, S. L. Jacques, and L. Zheng, “MCML-Monte-Carlo modeling of light transport in multi-layered tissue,” *Comput. Methods Programs Biomed.* **47**, 131–146 (1995).
 40. V. Tuchin, *Tissue Optics: Light Scattering Methods, and Instruments for Medical Diagnosis*, **TT 38**, SPIE Press, Bellingham, WA (2000).
 41. A. Aden, and M. Kerker, “Scattering of electromagnetic waves from two concentric spheres,” *J. Appl. Phys.* **22**, 1242–1246 (1951).
 42. See <http://diogenes.iwt.uni-bremen.de/vt/laser/codes/Mie-Matlab-Maetzler.zip>.
 43. A. Knüttel, and M. Bochlau-Godau, “Spatially confined, and temporally resolved refractive index, and scattering evaluation in human skin performed with optical coherence tomography,” *J. Biomed. Opt.* **5**, 83–92 (2000).
 44. G. Mie, “Beiträge zur optik über medien, speziell kolloidaler metallösungen,” *Ann. Phys.* **330**, 377–445 (1908).
 45. C. F. Bohren, and D. R. Huffman, *Absorption, and Scattering of Light by Small Particles*, Wiley, New York (1983).
 46. O. J. Glembocki, and H. Piller, *Handbook of Optical Constants of Solids*, E. D. Palik, Ed., p. 503, Academic Press, Orlando, FL (1985).
 47. R. P. Gupta, and T. F. Wall, “The complex refractive index of particles,” *J. Phys. D: Appl. Phys.* **14**, L95–8 (1981).